

000
001
002003

Texture Mapping 3D Models of Indoor Environments with Noisy Camera Poses

004
005
006
007
008
009
010
011012 Anonymous 3DIMPVT submission
013014 Paper ID ****
015016

Abstract

Automated 3D modeling of building interiors is useful in applications such as virtual reality and environment mapping. Applying textures to these models is an important step in generating photorealistic visualizations of data collected by modeling systems. Camera pose recovery in such systems often suffers from inaccuracies, resulting in visible discontinuities when different images are projected adjacently onto a plane for texturing. We propose two approaches for reducing discontinuities in texture mapping 3d models made of planar surfaces. The first one is tile based and can be used where camera axes are at arbitrary angles with respect to the plane normals of the surfaces. The second one results in a more seamless texture but is only applicable where camera axes for imagery are closely aligned with plane normals. The effectiveness of our approaches are demonstrated on two indoor datasets.

032

1. Introduction

Three-dimensional modeling of indoor environments has a variety of applications such as training and simulation for disaster management, virtual heritage conservation, and mapping of hazardous sites. Manual construction of these digital models can be time consuming, and as such, automated 3D site modeling has garnered much interest in recent years.

The first step in automated 3D modeling is the physical scanning of the environment's geometry. An indoor modeling system must be able to recover camera poses within an environment while simultaneously reconstructing the 3D structure of the environment itself [2, 6, 7, 8]. This is known as the simultaneous localization and mapping (SLAM) problem, and is generally solved by taking readings from laser range scanners, cameras, and inertial measurement units (IMUs) at multiple locations within the environment.

Mounting such devices on a human-carried platform provides unique advantages over vehicular-based systems on wheels in terms of agility and portability, but can also re-

sult in much larger localization error. As a result, common methods for texture mapping generally produce poor results.

In this paper, we present a number of approaches to texture mapping 3D models of indoor environments made of planar surfaces in the presence of uncertainty and noise in camera poses. In particular, we consider a human-operated backpack system with a number of laser range scanners as well as 2 cameras facing left and right, each equipped with fisheye lenses reaching an approximately 180° field of view. Considering that the human operator walks at about 1 meter/second, and images are captured at 5 Hz, there is a considerable amount of overlap between successive images.

With the laser scanners active, the human operator wearing the backpack takes great care to walk a path such that every wall in the desired indoor environment is traversed and scanned lengthwise at least once.

Using data collected by the onboard sensors and applying multiple localization and loop-closure algorithms [2, 7, 8], the backpack is then localized over its data collection period. This requires recovering the 6 degrees of freedom for the backpack as well as all its sensors, including the cameras mounted on it.¹ Once this is complete, the data from the laser range scanners is used to generate a 3D point cloud of the surrounding environment. Approximate normal vectors for each point in the point cloud are then calculated by gathering neighboring points within a small radius and processing them through principal component analysis. These normal vectors allow for the classification and grouping of adjacent points into structures such as walls, ceilings, floors, and staircases. A RANSAC algorithm is then employed to fit polygonal planes to these structured groupings of points, resulting in a fully planar model [10]. This model, consisting of multiple 2D polygonal planes in 3D space, along with the set of images captured by the backpack's cameras and their noisy 3D poses, can be considered the input to our texture mapping problem.

The remainder of the paper is organized as follows. Section 2 describes the general problem of texture mapping and

¹In this paper, we use the terms localization and pose recovery interchangeably, in that they both refer to recovering position and orientation.

054
055
056
057
058
059
060
061
062
063
064
065
066
067
068
069
070
071
072
073
074
075
076
077
078
079
080
081
082
083
084
085
086
087
088
089
090
091
092
093
094
095
096
097
098
099
100
101
102
103
104
105
106
107

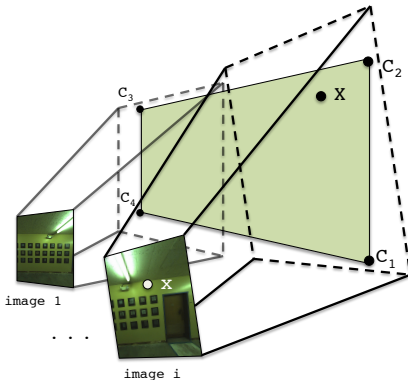
108
109
110
111
112
113
114
115
116
117
118
119
120

Figure 1: Planes are specified in 3D space by four corners C_1 to C_4 . Images are related to each plane through the camera matrices $P_{1..M}$.

examines two variants of a tile-based mapping approach and their shortcomings. Section 3 demonstrates two previous attempts at improving texture alignment, and demonstrates their inadequacies for our datasets. Section 4 presents our proposed approach to texture mapping, combining an improved localization refinement process with two image selection approaches. Section 5 contains results and conclusions.

In all subsequent sections, we discuss the process of texture mapping a single plane, as the texturing of each of our planes is independent and can be completed in parallel.

2. Tile-Based Texture Mapping

The geometry of the texture mapping process for a plane is shown in Figure 1. As described earlier, we are provided with a set of M images with which we must texture our target plane. Each image has a camera matrix P_i for $i = 1..M$, which translates a 3D point in the world coordinate system to a 2D point or pixel in image i 's coordinates. A camera matrix P_i is composed of the camera's intrinsic parameters, such as focal length and image center, as well as extrinsic parameters which specify the rotation and translation of the camera's position in 3D world coordinates at the time that image i is taken. These extrinsic parameters are determined by the backpack hardware and localization algorithms [2, 8, 7] and are quite noisy.

Our goal is to texture each plane using images captured by the backpack system, while eliminating any visual discontinuities or seams that would suggest that the plane's texture is not composed of a single continuous image.

2.1. Direct Mapping

Ignoring the fact that the camera matrices $P_{1..M}$ are inaccurate, we can texture the plane by discretizing it into small square tiles, generally about 5 pixels across, and choosing

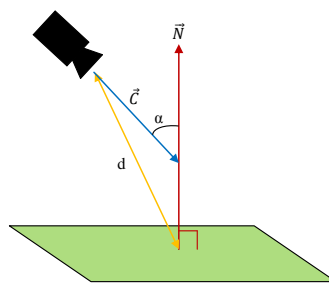
162
163
164
165
166
167
168
169
170
171
172
173
174

Figure 2: We wish to minimize camera angle α and distance d

an image to texture each tile with. We choose to work with rectangular units to ensure that borders between any two distinct images in our final texture are either horizontal or vertical. Since most environmental features inside buildings are horizontal or vertical, any seams in our texture intersect them minimally and are likely to be less noticeable.

In order to select an image for texturing tile t , we must first gather a list of candidate images that contain all four of its corners, which we can quickly check by projecting t into each image using the projection method above. Furthermore, each candidate image must have been taken at a time when its camera had a clear line-of-sight to t , which can be calculated using standard ray-polygon intersection tests between the camera location, the center of t , and every other plane, all in world coordinates [5].

Once we have a list of candidate images for t , we must define a scoring function in order to compare images and objectively select the best one. Since camera localization errors compound over distance, we wish to minimize the distance between cameras and the plane they texture. Additionally, we desire images that are projected perpendicularly onto the plane, maximizing the resolution and amount of useful texture available in their projections. In other words, we wish to minimize the angle between the plane normal and the camera axis for images selected for texture mapping. These two criteria can be met by maximizing the function $\frac{1}{d}(-1 \cdot \vec{C}) \cdot \vec{N}$ with the parameters shown in Figure 2. Specifically, d is the distance between the centers of a camera and a tile, and \vec{N} and \vec{C} are the directions of the plane's normal and the camera axis respectively.

As Figure 3(a) demonstrates, this approach leads to the best texture for each tile independently, but overall results in many image boundaries with abrupt discontinuities, due to significant misalignment between images, as a result of camera pose inaccuracies.

2.2. Mapping with Caching

Since discontinuities occur where adjacent tiles select non-aligned images that do not align, it makes sense to take into account image selections made by neighboring tiles

175
176
177
178
179
180
181
182
183
184
185
186
187
188
189
190
191
192
193
194
195
196
197
198
199
200
201
202
203
204
205
206
207
208
209
210
211
212
213
214
215

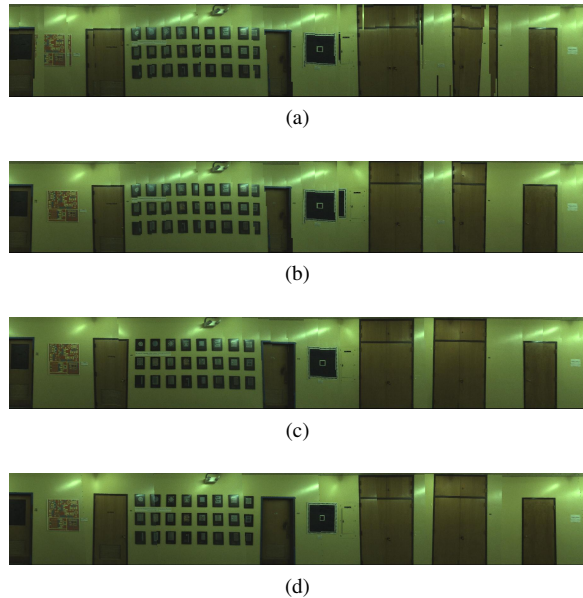


Figure 3: (a): Direct mapping. (b): Mapping with caching. (c): Mapping with caching after image alignment. (d): Seam minimization approach (including image alignment)

while selecting the best image for a given tile. By using the same image across tile boundaries, we can eliminate a discontinuity altogether. If this is not possible because a tile is not visible in images chosen by its neighbors, using similar images is likely to result in less noticeable discontinuities.

Similar to a caching mechanism, we select the best image for a tile t by searching through two subsets of images for a good candidate, before searching through the entire set. The first subset of images is those selected by adjacent tiles that have already been textured. We must first check which images can map to t , and then of those, we make a choice according to the same scoring function. Before reusing this image, we ensure it meets a threshold, which we set unconditionally to $\alpha < 45^\circ$, to be considered a viable image, with α as the camera angle as shown in Figure 2.

If no satisfactory image is found in the first subset, we then check our second subset of images, which consists of images that were taken near the images in the first subset, both spatially and temporally. These images are not the same as the ones used for neighboring tiles, but they were taken at a similar location and time, suggesting that their localization and projection are very similar. Again, if no good image is found according to the same threshold, we must then search the entire set of candidate images, selecting based on the criteria from Figure 2.

The results of this caching approach are shown in Figure 3(b). As compared to Figure 3(a), discontinuities are reduced overall, but the amount of remaining seams sug-

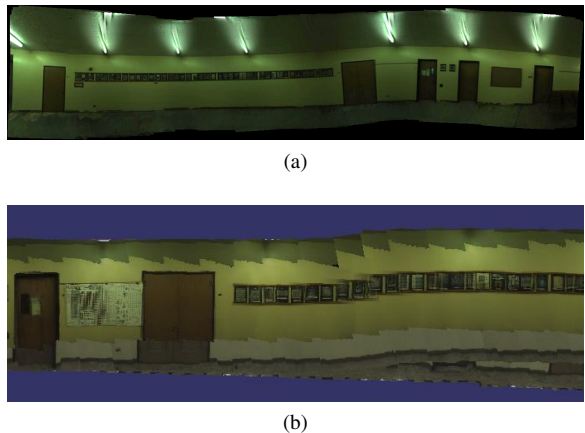


Figure 4: Both image mosaicing (a) and the graph-based localization refinement algorithm from [2] (b) suffer from the problem of compounding errors.

gests that image selection alone cannot produce seamless textures. Camera matrices, or the image projections themselves have to be adjusted in order to reliably generate clean textures.

3. Existing Approaches to Image-Aligned Texture Mapping

In order to produce seamless texture mapping, either camera matrices need to be refined such that their localization is pixel accurate, or image stitching techniques need to be applied to provide this illusion.

Before examining these approaches, we first obtain a set of images to work with. Rather than perform camera or image adjustments across the many thousands of images acquired in a typical data collection, we opt to work with the more limited set of images corresponding to those chosen by the direct mapping approach, without caching (Section 2.1). This set of images constitutes a good candidate set for generating a final seamless texture since it meets three important criteria. First, each tile on our planeis covered by at least one image in this set; this ensures no holes in our final texture. Second, images are all selected according to the scoring function in Figure 2, ensuring good camera distances and angles. Third, as a side result of the scoring function, selected images are only viable candidates for the tiles near their center of projection. Thus, there should be plenty of overlap between selected images, allowing for some degree of shifting without resulting in holes, as well as area for blending between them. With this set of images, we now review two existing approaches towards refining and combining their projections.

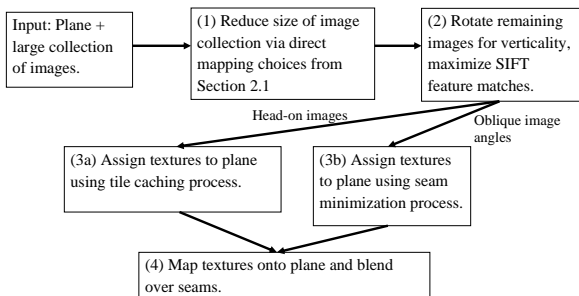


Figure 5: Our proposed method for seamless texture mapping.

3.1. Image Mosaicing

When images of a plane are taken from arbitrary overlapping positions, they are related by homography [6]. Thus, existing homography-based image mosaicing algorithms are applicable [1]. However, errors can compound when long chains of images are mosaiced together using these approaches. For example, a pixel in the n th image in the chain must be translated into the first image's coordinates by multiplying by the 3×3 matrix $H_1 H_2 H_3 \dots H_n$. Any error in one of these homography matrices is propagated to all further images until the chain is broken. For some chains of images this can happen almost immediately due to erroneous correspondence matches and the resulting image mosaic is grossly misshapen.

Figure 4(a) shows the output of the AutoStitch software package which does homography-based image mosaicing. This plane is nearly a best-case scenario with many features spread uniformly across it. Even so, the mosaicing produces errors that cause straight lines to appear as waves on the plane, despite the fact that it was generated after careful hand tuning. Many planes with fewer features simply failed outright. Thus, image mosaicing is not a robust enough solution for reliably texture mapping our dataset.

3.2. Image-Based 3D Localization Refinement

Another approach is to refine the camera matrices using image correspondences to guide the process. Each image's camera matrix has 6 degrees of freedom that can be adjusted. Previous work on this problem attempted to refine camera matrices by solving a non-linear optimization problem [8]. This process is specific to the backpack system which generated our dataset, as it must be run during backpack localization[8, 2]. This approach suffers from a similar error propagation problem as shown in Figure 4(b).

4. Proposed Method for Seamless Texture Mapping

In this section, we will describe our proposed method for seamless texture mapping. Our approach consists of 4 steps, as seen in Figure 5. First, we choose a subset of M images to work with via the direct mapping approach of Section 2.1. Next, we perform image rotation and shifting in order to maximize SIFT feature matches in overlapping areas between images. We then project these images onto our plane, applying textures either with the tile caching method from Section 2.2, or with the more specialized method to be described in Section 4.3. This choice depends on the availability of head-on images for a given plane. We then finish by applying linear alpha blending to smooth out any remaining seams.

4.1. Image Projection and Rotation

We begin with the projection of all images onto the plane. This is done in the same way as the approaches in Section 2. We then perform rotations on these projections, as adjacent images with different orientations result in strong discontinuities.

These rotations are accomplished by using Hough transforms, which detect the presence and orientation of linear features in our images. Rather than match the orientation of such features in each image, we simply apply rotations such that the strongest near-vertical features are made completely vertical. This is effective for vertical planes in indoor models, since they usually consist of parallel vertical lines corresponding to doors, wall panels, rectangular frames, etc. If features in the environment are not vertical, or are not parallel to each other, this step is skipped.

4.2. Image Pose Refinement

Our next step is to align overlapping images by searching for corresponding points between all pairs of overlapping images using SIFT feature matching [9]. The SIFT matches determine dx and dy distances between each pair of features for two images on the plane, though these distances may not always be the same for different features.

Since indoor environments often contain repetitive features such as floor tiles or doors, we need to ensure that our SIFT-based distances are reliable. In order to mitigate the effect of incorrect matches and outliers, the RANSAC framework [4] is used for a robust estimate of the optimal $dx_{i,j}$ and $dy_{i,j}$ distances between two images i and j . The RANSAC framework handles the consensus-building machinery, and requires a fitting function and a distance function. For this application, the fitting function simply finds the average distance between matches in a pair of images. The distance function for a pair of points is chosen to be the difference between those points' SIFT match distance

324	378
325	379
326	380
327	381
328	382
329	383
330	384
331	385
332	386
333	387
334	388
335	389
336	390
337	391
338	392
339	393
340	394
341	395
342	396
343	397
344	398
345	399
346	400
347	401
348	402
349	403
350	404
351	405
352	406
353	407
354	408
355	409
356	410
357	411
358	412
359	413
360	414
361	415
362	416
363	417
364	418
365	419
366	420
367	421
368	422
369	423
370	424
371	425
372	426
373	427
374	428
375	429
376	430
377	431

432 and the average distance computed by the fitting function;
 433 we use a 10 pixel outlier threshold. This means that a SIFT
 434 match is labeled as an outlier if its horizontal or vertical
 435 distance is not within 10 pixels of the average distance com-
 436 puted by the fitting function.
 437

We now use the $dx_{i,j}$ and $dy_{i,j}$ distances between each pair of images to refine their positions using least squares. Recall that there are a total of M^2 possible pairs of images, though we only generate distances between images that overlap at SIFT feature points. Given these distances and the original image location estimates, we can solve a least squares problem ($\min_{\vec{\beta}} \|A\vec{\beta} - \vec{\gamma}\|_2^2$) to estimate the location of the images on the plane. The M -dimensional vector $\vec{\beta}$ represents the unknown x location of each image on the plane for $1 \dots M$. The optimal x and y locations are obtained in the same way, so we only consider the x locations here:

$$\vec{\beta} = (x_1, x_2, x_3, \dots x_{M-1}, x_M)$$

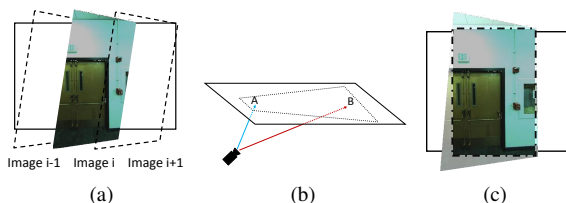
The $N \times (M + 1)$ dimensional matrix A is constructed with one row for each pair of images with measured distances produced by the SIFT matching stage. A row in the matrix has a -1 and 1 in the columns corresponding to the two images in the pair. For example, the matrix below indicates that we generated a SIFT-based distance between images 1 and 2, images 1 and 3, images 2 and 3, etc.

$$A = \begin{pmatrix} -1 & 1 & 0 & \dots & 0 & 0 \\ -1 & 0 & 1 & \dots & 0 & 0 \\ 0 & -1 & 1 & \dots & 0 & 0 \\ \vdots & \vdots & \vdots & \ddots & \vdots & \vdots \\ 0 & 0 & 0 & \dots & 1 & 0 \\ 0 & 0 & 0 & \dots & -1 & 1 \\ 1 & 0 & 0 & \dots & 0 & 0 \end{pmatrix}$$

If only relative distances between images are included then there is no way to determine the absolute location of any of the images and the matrix becomes rank deficient. To fix this we choose the first image to serve as the anchor for the rest, meaning all the absolute distances are based on its original location. This is done by adding a row with a 1 in the first column and the rest zeros.

Finally, the N -dimensional observation vector $\vec{\gamma}$ is constructed using the SIFT-based distances generated earlier in the RANSAC matching stage. The last element in the observation vector is the location of the first image determined by its original noisy localization, from [2, 8]. Thus $\vec{\gamma}$ can be written as:

$$\vec{\gamma}^T = (d_{1,2}, d_{1,3}, d_{2,3}, \dots d_{N-2,N-1}, d_{N-1,N}, x_1)$$



486
 487
 488
 489
 490
 491
 492
 493
 494
 495
 496
 497
 498
 499
 500
 501
 502
 503
 504
 505
 506
 507
 508
 509
 510
 511
 512
 513
 514
 515
 516
 517
 518
 519
 520
 521
 522
 523
 524
 525
 526
 527
 528
 529
 530
 531
 532
 533
 534
 535
 536
 537
 538
 539

Figure 6: (a): Undistorted fisheye images for vertical planes are tilted, but their effective camera axis is more or less normal to the plane. (b): The effective camera axis for ceilings is at an angle with respect to the plane normal. (c): Wall images are cropped to be rectangular.

The $\vec{\beta}$ that minimizes $\|X\vec{\beta} - \vec{\gamma}\|_2^2$ results in a set of image locations on the plane that best honors all the SIFT-based distance measurements between images. In practice there are often cases where there is a break in the chain of images, meaning that no SIFT matches were found between one segment of the plane and another. In this case we add rows to the A matrix and observations to the $\vec{\gamma}$ vector that contain the original noisy x and y distance estimates generated by the localization algorithm [2, 8]. Another way to do this is to add rows for all neighboring pairs of images and solve a weighted least squares problem where the SIFT distances are given a higher weight i.e. 1, and the noisy distances generated by the localization algorithm [2, 8] are given a smaller weight i.e. 0.01.

After completing this same process for the y dimension as well, and making the resultant shifts, our images overlap and match each other with far greater accuracy. Applying the tile caching method from Section 2.2 on these re-localized images results in the significant improvements shown in Figure 3(c), as compared to Figure 3(b).

4.3. Seam Minimization

As mentioned earlier, the mobile backpack system used to capture data in this paper contains 2 cameras with 180° fisheye lenses facing to the right and left. Since most human operators do not carry the backpack in a perfectly upright position and are bent forwards at 15 to 20 degrees with respect to the vertical direction, the undistorted fisheye images are head on with respect to vertical walls, but at an angle with respect to horizontal floors and ceilings. This is depicted in Figure 6.

These oblique camera angles translate into textures that span extremely large areas once projected. Using the tile-based texture mapping criteria from Figure 2, such projections have good scores for certain areas on the plane, but worse scores for others. The tiling approach in Section 2 is thus a good choice for texturing floors and ceilings, as it uses the parts of image projections that are good choices for their respective plane locations, e.g. areas near point A in

540

Figure 6(b), but not near point B.

541

For wall planes however, most images are taken from close distances and more or less head-on angles, resulting in higher resolution fronto-parallel projections. As a result, for each tile on a wall plane, the cost function of Figure 2 is relatively flat with respect to a large number of captured images, as they are all more or less head on. Thus it is conceivable to use a different texturing strategy for walls so as to minimize the visible seams for texture mapped planes. One way to do so is to choose the smallest possible set of images that (a) covers the entire plane and (b) minimizes the amount of visible seams. A straightforward cost function that accomplishes the latter is the sum of squared pixel differences in overlapping regions between all pairs of images, after they have been aligned as described in Section 4.1. Minimizing this cost function, which we refer to as SSD, encourages image boundaries to occur either in featureless areas, such as bare walls, or in areas where images match extremely well.

559

To cover the entirety of a plane, our problem can be defined as minimally covering a polygon i.e. the plane, using other polygons of arbitrary geometry i.e. image projections, with the added constraint of minimizing the cost function between chosen images. This is a complex problem, though we can take a number of steps to simplify it. Given that wall-texture candidate images are taken from more or less head-on angles, and assuming only minor rotations are made during localization refinement, we can reason that their projections onto the plane are approximately rectangular. By cropping them all to be rectangular, as shown in Figure 6(c), our problem becomes the conceptually simpler one of filling a polygon with rectangles, such that the sum of all costs between each pair of rectangles is minimal. We thus also retain the advantages of working with rectangular units, as explained in Section 2.

575

The location and orientation of the cameras on the acquisition backpack is such that images nearly always contain the entirety of the floor to ceiling range of wall planes. Images are therefore rarely projected with one above another when texturing wall planes. In essence, we need only to ensure horizontal coverage of wall planes, as our images provide full vertical coverage themselves. We can thus construct a Directed Acyclic Graph (DAG) from the images, with edge costs defined by the SSD cost function, and solve a simple shortest path problem to find an optimal subset of images with regard to the cost function [3].

587

Figure 7 demonstrates the construction of a DAG from overlapping images of a long hallway. Images are sorted by horizontal location left to right, and become nodes in a graph. Directed edges are placed in the graph from left to right between images that overlap. The weights of these edges are determined by the SSD cost function. Next, we add two artificial nodes, one start node representing the left

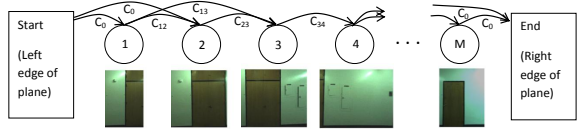


Figure 7: DAG construction for the image selection process.

594

595

596

597

598

599

600

601

602

603

604

605

606

607

608

609

610

611

612

613

614

615

616

617

618

619

620

621

622

623

624

625

626

627

628

629

630

631

632

633

634

635

636

637

638

639

640

641

642

643

644

645

646

647

border of the plane, and one end node representing the right border of the plane. The left(right) artificial node has directed edges with equal cost C_0 to(from) all images that meet the left(right) border of the plane.

We now solve the shortest path problem from the start node to the end node. This provides a set of images completely covering the plane horizontally, while minimizing the cost of seams between images.

In rare cases where the vertical dimension of the plane is not entirely covered by one or more chosen images, we are left with holes where no images are selected to texture. To address this, we solve for a new shortest path after modifying the edges chosen by the original shortest path solution such that they have higher cost than all other edges in our DAG, and solve for a new shortest path. This ensures that these edges are not chosen again unless they are the only available option. Our second shortest path solution results in a new set of chosen images, of which we only retain those that cover areas not covered by the first set. This process can be repeated as many times as needed, until holes are no longer present. This method is not as optimal as a 2D-coverage solution would be, but it is a fast approximation, and adequately handles the few holes we encounter.

With this completed, we have now mapped every location on the plane to at least one image, and have minimized the number of images, as well as the discontinuities between their borders. Figures 3(c) and 3(d) compare the tile caching method against this seam minimization method. For the latter, we arbitrarily choose one image for texturing where images overlap. Though both methods provide aligned texturing, the seam minimization approach results in fewer visible discontinuities, since it directly reduces the cost of each image boundary, while the tile caching method uses a scoring function that only approximates this effect. Furthermore, seam minimization guarantees the best selection of images, while the sequential tile caching method may select images early on that turn out to be poor choices once subsequent tiles have been processed. The seam minimization approach is also less intensive in terms of memory usage and runtime, as it does not require discretizing planes or images.

In the context of texturing an entire 3D planar model, we apply the seam minimization approach on walls, due to its superior output when provided with head-on images. Floors and ceilings however, given their many images taken at oblique angles, are textured using the tile caching method.

648
649
650
651
652
653
654
655

(1) Direct Mapping

656
657
658
659
660
661
662
663
664

(2) Direct Mapping after Image Adjustment

665
666

(3a) Tile Caching after Image Adjustment

667
668
669
670
671
672
673

(3b) Seam Minimization after Image Adjustment

674
675
676

(4a) Tile Caching after Image Adjustment, Blending

677
678
679

(4b) Seam Minimization after Image Adjustment, Blending

Figure 8: Textures corresponding to each step in our texture mapping pipeline.

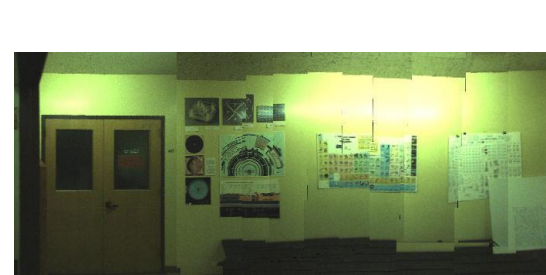
702
703
704
705
706
707
708
709710
711
712
713
714
715
716
717
718719
720
721
722
723
724
725
726
727728
729
730731
732
733734
735
736
737738
739
740
741
742
743

4.4. Blending

We now apply the same blending process to the two texturing methods: localization refinement followed by either tile caching or seam minimization.

Although the preprocessing steps and image selection in both methods attempt to minimize all mismatches between images, there are occasional unavoidable discontinuities in the final texture due to different lighting conditions or inaccuracies in planar geometry or projection. These can however be treated and smoothed over by applying alpha blending over image seams. Whether the units we are blending are rectangularly-cropped images or rectangular tiles, we can apply the same blending procedure, as long as we have a guaranteed overlap between units to blend over.

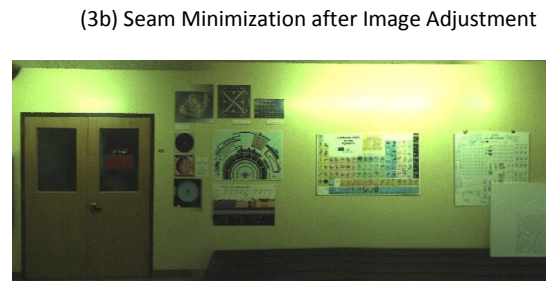
For the tile caching method, we can ensure overlap by texturing a larger tile than needed for display. For example, for a rendered tile $l_1 \times l_1$, we can associate it with a texture $(l_1 + l_2) \times (l_1 + l_2)$ in size. For the seam minimization method, we have already ensured overlap between images. To enforce consistent blending however, we add a minimum required overlap distance while solving the



(1) Direct Mapping



(2) Direct Mapping after Image Adjustment



(3a) Tile Caching after Image Adjustment



(3b) Seam Minimization after Image Adjustment



(4b) Seam Minimization after Image Adjustment, Blending

shortest path problem in Section 4.3. Additionally, if images overlap in a region greater than the overlap distance, we only apply blending over an area equal to the overlap distance.

After blending pixels linearly across overlapping regions using alpha blending, texture mapping is complete. Figure 8 shows each incremental step of our texture mapping approach for a different wall, as well as the final blended output resulting from both of our methods.

5. Results and Conclusions

In this paper, we have developed an approach to texture map models with noisy camera localization data. We are able to refine image locations based on feature matching, and robustly handle outliers. The tile-based mapping approach can be used to texture both simple rectangular walls as well as complex floor and ceiling geometry. We also presented a seam minimization texturing method that produces seamless textures on planes where multiple head-on images are available. Each of these approaches is highly modular, and easily tunable for different environments and acquisi-

756

tion hardware.

757

Examples of ceilings and floors textured with the tile caching approach, and walls textured with the seam minimization approach, are displayed in Figure 9. High resolution texture comparisons, as well as a walkthrough of a fully textured 3D model are available in the accompanying video to this paper.

763

References

764

- [1] M. Brown and D. Lowe. Automatic panoramic image stitching using invariant features. *International Journal of Computer Vision*, 74(1):59–73, 2007. 4
- [2] G. Chen, J. Kua, S. Shum, N. Naikal, M. Carlberg, and A. Zakhor. Indoor localization algorithms for a human-operated backpack system. In *Int. Symp. on 3D Data, Processing, Visualization and Transmission (3DPVT)*. Citeseer, 2010. 1, 2, 3, 4, 5
- [3] E. Dijkstra. A note on two problems in connexion graphs. *Numerische Mathematik*, 1:269–271, 1959. 6
- [4] M. Fischler and R. Bolles. Random sample consensus: a paradigm for model fitting with applications to image analysis and automated cartography. *Communications of the ACM*, 24(6):381–395, 1981. 4
- [5] A. Glassner et al. *An introduction to ray tracing*. Academic Press, 1989. 2
- [6] R. Hartley and A. Zisserman. *Multiple view geometry in computer vision*, volume 2. Cambridge Univ Press, 2000. 1, 4
- [7] J. Kua, N. Corso, and A. Zakhor. Automatic loop closure detection using multiple cameras for 3d indoor localization. In *IS&T/SPIE Electronic Imaging*, 2012. 1, 2
- [8] T. Liu, M. Carlberg, G. Chen, J. Chen, J. Kua, and A. Zakhor. Indoor localization and visualization using a human-operated backpack system. In *Indoor Positioning and Indoor Navigation (IPIN), 2010 International Conference on*, pages 1–10. IEEE, 2010. 1, 2, 4, 5
- [9] D. Lowe. Object recognition from local scale-invariant features. In *Computer Vision, 1999. The Proceedings of the Seventh IEEE International Conference on*, volume 2, pages 1150–1157. Ieee, 1999. 4
- [10] V. Sanchez and A. Zakhor. Planar 3d modeling of building interiors from point cloud data. In *International Conference on Image Processing*, 2012. 1

798

A. Occlusion Masking

799

For the seam minimization process, we need to ensure that our images contain only content that should be mapped onto the target plane in question. The tiling approach only checks occlusion for each tile as it is being textured. For seam minimization, entire images are used, so occlusion checks need to be performed over the entirety of each image to determine available areas for texture mapping.

807

Fortunately, by virtue of our indoor environments, the vast majority of surface geometry is either horizontal or vertical, with high amounts of right angles. This means that



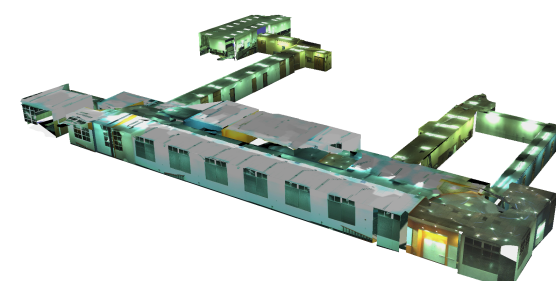
(a)



(b)



(c)



(d)

810

811

812

813

814

815

816

817

818

819

820

821

822

823

824

825

826

827

828

829

830

831

832

833

834

835

836

837

838

839

840

841

842

843

844

845

846

847

848

849

850

851

852

853

854

855

856

857

858

859

860

861

862

863

after masking out occluded areas, image projections will remain largely rectangular. We can be efficient by recursively splitting each image into rectangular pieces, and performing the same occlusion checks used in the tiling process where

864 needed. To occlude out rectangles, their texture is removed, 918
865 as untextured areas are never used for texture mapping. 919
866 920
867 921
868 922
869 923
870 924
871 925
872 926
873 927
874 928
875 929
876 930
877 931
878 932
879 933
880 934
881 935
882 936
883 937
884 938
885 939
886 940
887 941
888 942
889 943
890 944
891 945
892 946
893 947
894 948
895 949
896 950
897 951
898 952
899 953
900 954
901 955
902 956
903 957
904 958
905 959
906 960
907 961
908 962
909 963
910 964
911 965
912 966
913 967
914 968
915 969
916 970
917 971